

1 **Airborne laser scanning transects over Canada's northern** 2 **forests: lidar plots for science and application**

3 Christopher W. Bater¹, Joanne C. White¹, Hao Chen¹, Piotr Tompalski¹, Txomin Hermosilla¹,
4 Michael A. Wulder¹

5 ¹Canadian Forest Service (Pacific Forestry Centre), Natural Resources Canada, 506 West Burnside Road, Victoria,
6 British Columbia, Canada

7 *Correspondence to:* Christopher W. Bater (christopher.bater@nrcan-rncan.gc.ca)

8 **Abstract** Mapping vegetation is required for monitoring the condition of forest resources. Satellite data provide
9 information on land cover and change; however, forest structural attributes are difficult to model without additional
10 measurements from ground plots or airborne laser scanning (ALS, also known as airborne light detection and
11 ranging or lidar) instruments. Over large and inaccessible areas, such as Canada's northern and predominantly
12 unmanaged forests, ground plots are expensive, difficult to install, and unlikely to form a statistically valid
13 probability sample. An alternative means to obtain information regarding forest structure in these situations is
14 samples of ALS (hereafter lidar plots). Transect-based samples of ALS data can be used to provide structural
15 information for the calibration and validation of spatially explicit predictive modelling for wide-area mapping of
16 forest attributes. Here we describe and share data from the recent acquisition and processing of ALS transects across
17 Canada's northern forests. ~~To date, approximately 43,000~~Approximately 55,000 km of ALS transects have been
18 acquired in 2023, ~~and 2024,~~ and 2025 with additional coverage ongoing for 2025. Acquisition specifications
19 included minimum swath widths of 500 m (year 2023) or 800 m (2024 and 2025), with a minimum pulse density of
20 12 pulses/m². Acquisition flight lines were designed to sample a range of northern forest conditions and to
21 correspond with a concurrent ground plot sampling campaign. Airborne laser scanning data were processed into
22 height-normalized point clouds and reprojected to a custom Lambert conformal conic projection to align with
23 existing national satellite information products. More than 15 million 900 m² lidar plots were generated from the
24 2023 transect dataset with point cloud metrics (i.e., area-based statistical summaries of the ALS point cloud)
25 calculated for each 30 by 30 m cell. Presently, the 2023 lidar plots and their associated point cloud metrics are stored
26 in openly available SQLite GeoPackages, with additional annual transect collections to be added as available. To
27 accommodate a wide range of users and applications, both comprehensive and abridged versions of the metric
28 databases, with 369 metrics and 40 metrics, respectively, are shared. The framework underlying this dataset is fully
29 transferable to other regions with comparable information needs. The flexible data structure used allows seamless
30 integration of additional open-access ALS transect data as new acquisitions and processing become available. By
31 providing detailed, scalable measurements that bridge the gap between ground observations and wall-to-wall
32 satellite information products, this open-access resource empowers both the scientific and operational forestry
33 communities. These data will drive the development of enhanced wildfire fuels maps, comprehensive forest

34 inventories, and robust carbon products, supporting informed decision making and advancing sustainable forest
35 management.

36 **1 Introduction**

37 Vegetation structure underpins a range of ecological, social, and economic forest values, including timber
38 harvesting, carbon sequestration, biodiversity, water quality, and wildfire fuels (Haslem et al., 2011; Keith et al.,
39 2009; Tews et al., 2004). Medium resolution satellite remote sensing (i.e., pixels sided 10 – 100 m) has proven
40 effective for the wall-to-wall mapping of land cover (Hermosilla et al., 2022; Vogelmann et al., 2001), monitoring
41 disturbance and recovery (Hansen et al., 2014; White et al., 2017b), and more recently modelling attributes such as
42 species (Hermosilla et al., 2024). The characterization of vegetation structure, however, can be modeled using pixel-
43 based, optical remotely sensed data (Coops et al., 2021), but not with the accuracies possible using light detection
44 and ranging (lidar) technologies, particularly airborne laser scanning (ALS). It is not entirely fair to compare optical
45 satellite remote sensing and ALS due to their differences in data costs to the end user, the level of detail captured,
46 and the intensity and repeatability of collection (Fassnacht et al., 2024). However, ALS provides access to
47 simultaneous measurements of the vertical distribution of vegetation and the underlying terrain morphology (Lefsky
48 et al., 2002), providing critical information on forest complexity and condition that cannot be obtained through other
49 remote sensing methods.

50 Investigations related to ALS and forest measurement have been ongoing since the 1980s (Aldred and Bonnor, 1985;
51 Nelson, 2013), and by the early 2000s the technology was recognized as a robust tool for estimating inventory
52 attributes related to vegetation structure (Næsset, 2004; Reutebuch et al., 2005; Wulder et al., 2008). Given the high
53 cost and limited access to airborne lidar instruments in the early years, many initial investigations adopted
54 probability sampling approaches to efficiently obtain representative data (Wulder et al., 2012b). In contrast, today
55 many Canadian jurisdictions are actively collecting wall-to-wall ALS data to support the development of enhanced
56 forest inventories; however, data acquisitions are typically focused on managed forests in the south, leaving remote,
57 northern forests underrepresented (White et al., 2025). Stinson et al. (2019) define forest management status in
58 Canada using ownership, protection status, and tenure as these three characteristics are "...related to forest
59 management interests, governance and objectives in a generalized way across all Canadian jurisdictions" (p. 103).
60 Definitions of managed forest are different for carbon accounting purposes wherein unmanaged forests are excluded
61 from reporting requirements (Ogle et al., 2018). Although they are not actively managed, northern forests are critical
62 to the aforementioned forest values. The federal government reports on all forests, both managed and unmanaged, as
63 implemented through the National Forest Inventory program and communicated via the annual State of the Forests
64 report (Natural Resources Canada, 2023). As Canada's mean annual temperature has increased at more than twice
65 the global rate (Bourdeau-Goulet and Hassanzadeh, 2021), northern forests are particularly vulnerable to increased
66 wildfire risk (Burton, 2023; Parisien et al., 2023), further underscoring the need to improve available information for
67 these forests.

68 Although typically flown in a wall-to-wall configuration, ALS data may be collected as sampled linear transects to
69 extend structural information over remote areas where continuous, wall-to-wall coverage is impractical. Wulder et
70 al. (2012b) described lidar sampling as a cost-effective alternative to wall-to-wall lidar acquisition for large-area
71 forest monitoring. The authors demonstrated that statistically sound sampling and inference methods can enable
72 robust characterizations of forest structure, and that integration of lidar samples with field and satellite data can
73 enhance scalability and precision of estimates. For example, Andersen et al. (2011) presented a methodology for
74 estimating forest biomass over a large area of interior Alaska. The authors used a combination of ground plots and
75 sampled ALS transects to achieve reasonable precision, underscoring the cost-efficiency of integrating partial
76 airborne lidar coverage. Also working in Alaska, Babcock et al. (2018) demonstrated that sparse lidar transects,
77 when fused with field plots and Landsat tree cover in a Bayesian geostatistical framework, can yield wall-to-wall
78 biomass maps with quantified uncertainty. Nelson et al. (2012) used an airborne profiling lidar to estimate forest
79 biomass in Norway and found that the results were similar to those obtained through ground surveys. Building on
80 this logic, Margolis et al. (2015) employed a three-phase sampling design combining ground plots, airborne
81 profiling lidar, and ICESat-GLAS satellite lidar data to estimate biomass across the North American boreal forest.

82 Wulder et al. (2012a) proposed the concept of lidar plots, wherein lidar transect data, augmented by ground plot
83 information, provide sample-based characterizations of forest structure. Lidar plot locations are established within
84 sampled lidar transect swaths at a spatial resolution matching the typical size (area) of tall tree ground plots or the
85 pixel size of medium spatial resolution remotely sensed data (e.g., pixels sized 400-900 m²). The ALS data are
86 processed to generate a suite of summary statistics or metrics that characterize the point cloud within each lidar plot
87 (e.g., mean height, maximum height, percentiles of height). Using an area-based approach (ABA) (Næsset, 2002;
88 White et al., 2013), a sample of co-located ground plot measurements are then used with the point cloud metrics to
89 generate predictions of inventory attributes of interest such as height, basal area, volume, or biomass, among others.
90 These lidar plots, with associated metrics and attributes, may then be linked to other remotely sensed data (e.g.,
91 optical time series) via imputation, enabling the generation of spatially exhaustive and spatially explicit models of
92 forest structure ultimately resulting in maps representing large areas (Coops et al., 2021; Wulder et al., 2012a).

93 In a proof-of-concept study, Zald et al. (2016) demonstrated how lidar plots could be used as a surrogate for ground
94 plots to map a suite of point cloud height (mean, standard deviation, coefficient of variation, 95th percentile) and
95 cover metrics (percentage of first returns > 2 m, percentage of first returns > mean height), as well as select forest
96 inventory attributes (Lorey's tree height, basal area, gross stem volume, and total aboveground biomass) for a ~38
97 million ha forest region in Saskatchewan, Canada for the year 2010 (corresponding to the year of ALS acquisition).
98 Zald et al. (2016) availed upon 1,560 km of lidar transects and a set of 4,340 lidar plots to impute point cloud
99 metrics directly, with the ABA forest attributes carried as ancillary variables in the plot-matching process.

100 Expanding on this approach, Matasci et al. (2018a) employed >25,000 km of lidar transects and 80,687 lidar plots
101 with Landsat surface reflectance composites to produce boreal-wide maps (~552 million ha) of the same point cloud
102 metrics and forest structural attributes as Zald et al. (2016) for the year 2010. Matasci et al. (2018b) further extended
103 this approach in both space and time, mapping forest structure annually for the entirety of Canada's forested

104 ecosystems (~650 million ha) for each year from 1984 to 2016. Matasci et al. (2018b) availed upon seven different
105 lidar acquisitions and associated lidar plots (n = 84,482) to achieve national, annual maps of forest structure, thereby
106 enabling characterization of structural dynamics in both disturbed and undisturbed forests over the three-decade
107 period considered. Matasci et al. (2018b) also used a completely independent set of lidar plots, derived from
108 separate lidar acquisitions to validate the imputed attributes, both spatially and temporally. Collectively, these
109 studies demonstrate the utility of ALS sampling and lidar plots in generating spatially and temporally rich forest
110 structural information at landscape to continental scales.

111 **1.1 Motivation**

112 Canada's boreal forests and the communities therein are increasingly exposed to wildfire risks (Parisien et al., 2020),
113 yet many northern and remote regions lack detailed vegetation inventories essential for fire behavior modeling
114 (Crowley et al., 2023; Parisien et al., 2020; Stinson et al., 2019). In these areas outside of the managed forest zone,
115 accurate information on forest structure and fuel properties is limited, constraining the capacity to assess risk or plan
116 mitigation strategies (Crowley et al., 2023). Further, the ongoing development of the next generation Canadian
117 Forest Fire Danger Rating System (CFFDRS-2025) will incorporate new data sources and requires that a new suite
118 of vegetation and soil attributes be modelled (Canadian Forest Service Fire Danger Group, 2021). Addressing this
119 data gap requires spatially explicit maps of key forest structural attributes such as canopy bulk density and canopy
120 base height which may be estimated using ALS (Andersen et al., 2005; Martin-Ducup et al., 2025; Moran et al.,
121 2020; Riaño et al., 2004), but cannot be reliably derived from satellite imagery alone (Mutlu et al., 2008; Riaño et
122 al., 2003) and which are equally difficult to estimate in the field (Keane et al., 2005).

123 To support this need, the Government of Canada via the Canadian Forest Service launched the Northern Forest
124 Mapping program (NorthForM). Between 2023 and 2025, this initiative is acquiring ALS transects and coincident
125 ground plot data (Boucher et al., 2023), with the goal of modeling fuel-related forest structure attributes for wall-to-
126 wall mapping using satellite imagery (Coops et al., 2021). These methods build upon earlier work by the National
127 Terrestrial Ecosystem Monitoring System (NTEMS), which was developed to monitor Canada's forested ecosystems
128 on an annual basis using consistent, nationally available datasets (White et al., 2014; Wulder et al., 2024). The
129 NTEMS relies primarily on medium spatial resolution satellite data (initially solely Landsat, now augmented with
130 Sentinel 2) time series, integrated with ALS transects and ground plots, to generate national information products
131 characterizing disturbance, land cover, and forest structure (Hermosilla et al., 2016). The first national lidar transect
132 dataset was collected in 2010 to support NTEMS product development (Hopkinson et al., 2011; Wulder et al.,
133 2012a), and subsequent work has shown that combining these data sources enables spatially comprehensive
134 estimates of both forest structure and derived attributes (Matasci et al., 2018a, b; Zald et al., 2016)

135 **1.2 Objectives**

136 Herein, we describe the acquisition and processing of ALS transect data for Canada's northern forests, and the
137 subsequent generation of 30 m lidar plots and ABA point cloud metrics. These data are being shared in an open

138 repository to support the development of models needed for generating wall-to-wall predictions of attributes relevant
139 for characterizing forest structure and informing forest fuels mapping.

140 **2 Data and methods**

141 **2.1 Canada's northern forests**

142 Canada's unmanaged northern forests represent some of the largest natural treed ecosystems on Earth. Spanning
143 northern Quebec, Ontario, Manitoba, Saskatchewan, Alberta, and significant portions of the Yukon and Northwest
144 Territories, they are mostly free of large-scale industrial land uses such as forestry. Unlike managed forests to the
145 south, these ecosystems are shaped primarily by natural disturbances such as wildfires and insect outbreaks,
146 although the anthropogenic footprint is expanding in some areas (Wells et al., 2020). Tree species are cold-tolerant,
147 primarily within the genera *Abies*, *Larix*, *Picea*, and *Pinus*, but also include *Populus* and *Betula*. Northern forests
148 and treed areas are part of a larger mosaic which includes lakes, rivers, and wetlands, treeless alpine areas, maritime
149 heathlands, and occasional grasslands (Brandt, 2009).

150 **2.2 Airborne laser scanning data acquisitions**

151 Planning for the 2023-2025 lidar acquisition considered previous experience with national ALS transects
152 (Hopkinson et al., 2011), as well as recommendations from the Canadian airborne lidar acquisition guidelines (CSA
153 Group, 2025). Acquisition specifications are summarized in Table 1. Due to the remoteness of the area of interest
154 (Figure 1), the lack of permanent global navigation satellite system (GNSS) base station infrastructure, and the
155 impracticality of setting up ad hoc base stations, precise point positioning (PPP) services were employed to correct
156 ALS return coordinates. The target window for data acquisition was between 15 June and 15 September of each
157 year, and linear mode lidar systems were required. The ALS data were collected by private sector vendors who were
158 awarded contracts through the Government of Canada's competitive procurement process (Table 2). Each vendor
159 used their own aircraft, sensors, and systems to collect data according to the specifications outlined in Table 1.

160

161

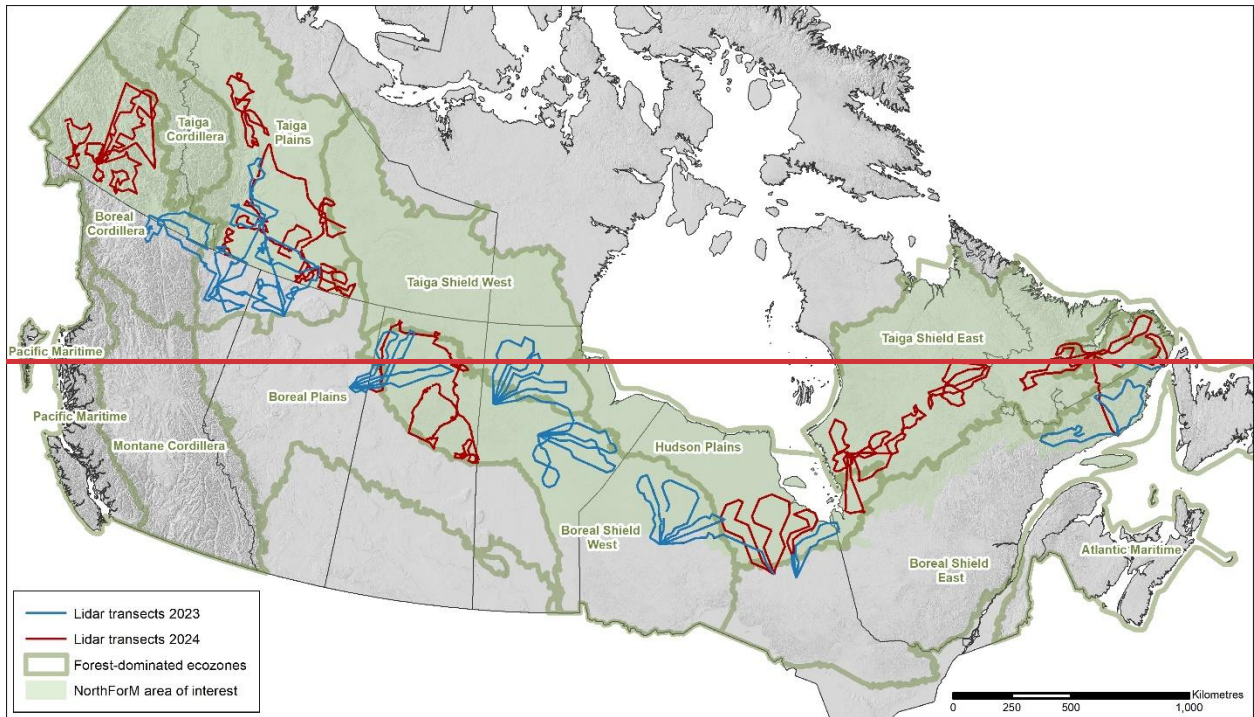
Table 1. Summary of ALS acquisition specifications for the 2023-2025 acquisition program.

Requirement	Acquisition 2023–2025
Aggregate nominal pulse density (ANDP)	12 pulses/m ²
Aggregate nominal pulse spacing (ANPS)	0.29 m
Footprint diameter	0.30 m
Scan angle	+/-20 degrees on either side of nadir (40 degrees total field of view)
Horizontal datum	NAD 83 CSRS epoch 2010
Height reference	Vertical datum: CGVD 2013 Geoid model: CGG2013a
Map projection	Universal Transverse Mercator (UTM)
Pulse returns	Multiple
Classification	1 – Processed but unclassified 2 – Ground 3 – Low vegetation 4 – Medium vegetation 5 – High vegetation 7 – Low points (noise) 9 – Water 18 – High noise
Intensity Value	Normalized 16-bit values, according to the method described in the ASPRS LAS 1.4 R15 specification.
Data Format	LAS 1.4 R-15, Point data record format 6, compressed in LAZ
Swath width	500 m (2023) or 800 m (2024 and 2025)

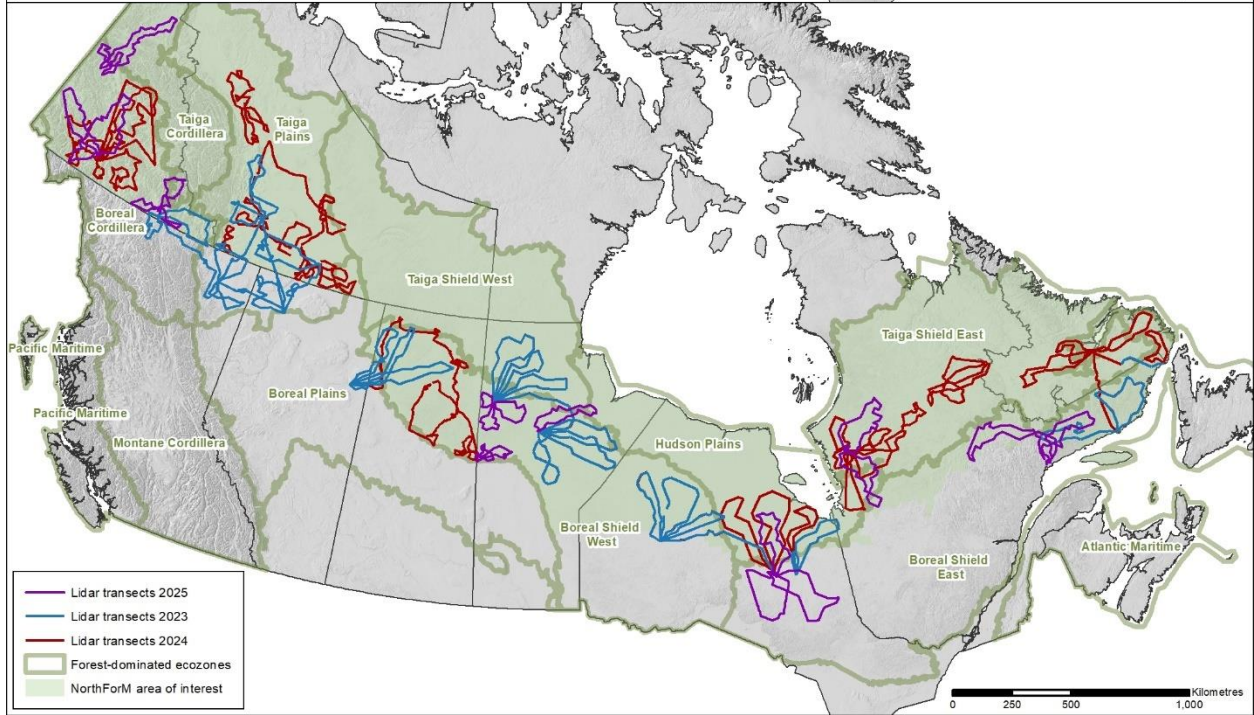
162

163

164



165



166

Figure 1. Airborne laser scanning (ALS) transects flown in 2023 (~20,000km), 2024 (~23,000 km), and 2025 (~12,000 km). The Northern Forest Mapping (NorthForM) acquisitions were largely focused on northern ecozones to improve mapping in unmanaged forests. Figure 1. Airborne laser scanning (ALS) transects flown in 2023 (~20,000km) and 2024 (~23,000 km). The Northern Forest Mapping (NorthForM) acquisitions are limited to northern ecozones to improve mapping in unmanaged forests.

168

169

170

171

172 **Table 2. Airborne lidar vendors for acquisition years 2023, and 2024, and 2025. Each lidar plot (described in section 2.4) is**
 173 **linked to acquisition information in a relational database.**

<u>Acquisition year</u>	<u>Vendor</u>	<u>Lidar sensor</u>
<u>2023</u>	<u>Aeroquest Mapcon</u>	<u>Riegl VQ-1560II-S</u>
	<u>Eagle Mapping</u>	<u>Riegl VQ-780II-S & Riegl VQ-1560II-S</u>
<u>2024</u>	<u>Aeroquest Mapcon</u>	<u>Riegl VQ-1560 II-S</u>
	<u>Eagle Mapping</u>	<u>Riegl VQ-780II-S & Riegl VQ-1560II-S</u>
	<u>McElhanney</u>	<u>Leica TerrainMapper-2</u>
<u>2025</u>	<u>Aeroquest Mapcon</u>	<u>Riegl VQ-1560 II-S</u>
	<u>Kisik</u>	<u>Riegl VQ-1560 II-S</u>

174
175

<u>Acquisition year</u>	<u>Vendor</u>	<u>Lidar sensor</u>
<u>2023</u>	<u>Aeroquest Mapeon</u>	<u>Riegl VQ-1560II-S</u>
	<u>Eagle Mapping</u>	<u>Riegl VQ-780II-S & Riegl VQ-1560II-S</u>
<u>2024</u>	<u>Aeroquest Mapeon</u>	<u>Riegl VQ-1560II-S</u>
	<u>Eagle Mapping</u>	<u>Riegl VQ-780II-S & Riegl VQ-1560II-S</u>
	<u>McElhanney</u>	<u>Leica TerrainMapper-2</u>

176

177 Canada’s National Forest Inventory (NFI) employs a systematic sampling strategy based upon 2 km x 2 km photo
 178 plots established on a 20 x 20 km grid, with the intent to sample 1% of Canada’s landmass. The 20 x 20 km sample
 179 grid is in turn nested within a 4 x 4 km system (Gillis et al., 2005). Candidate NorthForM ground plot locations were
 180 selected using a stratified sampling strategy employing sampling units that combined ecozone (Figure 1), and
 181 satellite-derived percent conifer and canopy closure obtained from the Spatialized Canadian National Forest
 182 Inventory (Guindon et al., 2024). Ground plot locations were then selected using the NFI’s 4 x 4 km sampling
 183 framework. Together, the NFI photo plot and NorthForM ground plot networks were used to guide ALS transect
 184 design, with plot centres used as targets between which lidar data were acquired. Additional ALS transects were
 185 established in an effort to obtain a balanced sample across northern forest-dominated ecozones where access was
 186 possible (Figure 1).

187 **2.3 Data processing**

188 **2.3.1 Point cloud processing**

189 Following their delivery by the ALS vendors, subsequent processing of the point cloud data was performed using
 190 LAStools (version 2.0.4; rapiddlasso GmbH). Footprint polygons were first created for each point cloud tile; the
 191 footprints followed the exterior edges of ALS returns and captured large internal voids. Classified lidar point clouds

192 were then normalized to obtain heights above ground, with returns less than 0 m and greater than 100 m being
193 removed. Returns with scan angles exceeding 20 degrees or classified as high noise (class 18) were dropped from
194 the point clouds (Table 1). The point clouds were then reprojected from their universal transverse Mercator (UTM)
195 projections (Table 1) to a common national Lambert conformal conic projection employed by the NTEMS program
196 (Table 3). The normalized and reprojected point clouds were then used to calculate point cloud metrics.

197 **Table 3. Projection information for National Terrestrial Ecosystem Monitoring System (NTEMS) spatial data: a custom**
 198 **Lambert conformal conic projection with two standard parallels using the NAD83 horizontal datum. Lidar plots were**
 199 **generated using this projection.**

Projection information	Projected coordinate system	Lambert Conformal Conic 2SP
	Projection	Lambert conformal conic
	Authority	Custom
	Linear unit	Metre (1.0)
	False easting	0
	False northing	0
	Central meridian	-95.0 degrees
	Standard parallel 1	49.0 degrees
	Standard parallel 2	77.0 degrees
Geographic coordinate system information	Latitude of origin	49.0 degrees
	Geographic coordinate system	NAD 1983
	WKID	4269
	Authority	EPSG
	Angular unit	Degree (0.0174532925199433)
	Prime meridian	Greenwich (0.0)
	Horizontal datum	North American 1983
	Spheroid	GRS 1980
	Semimajor axis	6378137.0
Semiminor axis	6356752.314140356	
Inverse flattening	298.257222101	

200

201 2.3.2 Lidar plots and point cloud metrics

202 Lidar plots and the databases in which they are stored were created using Python and ESRI's ArcPy package. Lidar
 203 plots were generated as point feature classes falling within the lidar transect swaths. Using the point cloud footprints,
 204 lidar plots were located away from the edges of swaths and large interior voids to avoid areas of missing data. The
 205 lidar plot centre coordinates aligned with the pixel centres of 30 m spatial resolution NTEMS raster products, which
 206 use the NTEMS Lambert conformal conic projection (Table 3). Plots that fell within the NTEMS land cover
 207 product's water class (Hermosilla et al., 2022) were removed. For each lidar plot, an individual 30 m x 30 point
 208 cloud was then clipped from which area-based metrics would be calculated in subsequent steps.

209 Lidar point cloud metrics were calculated for each 30 m x 30 m lidar plot using the R packages lidR (Roussel et al.,
 210 2020; Roussel and Auty, 2023) and lidRmetrics (Tompalski, 2024). As the final products are intended to inform a
 211 variety of applications, including forest inventory, regeneration assessment, and wildfire fuels, the metrics were
 212 generated in four groups using: (1) all returns above 0 m, (2) first returns above 0 m, (3) all returns above 2 m, and
 213 (4) first returns above 2 m. Two height thresholds were used so that models could be created that either consider all
 214 vegetation from the ground surface upwards (i.e., ≥ 0 m), or with a focus on overstory structure (> 2 m). Metrics
 215 were calculated using only first returns as they have been shown to be more consistent than metrics based on all
 216 returns (Bater et al., 2011); however, metrics considering all returns provide a more comprehensive characterization
 217 of vertical forest structure and may be preferred for applications that consider more than just the upper canopy
 218 (Singh et al., 2016). Each group included the same set of metrics, but values varied based on the combination of
 219 height threshold (0 m or 2 m) and return type (all returns or first returns only). In total, 369 point cloud metrics were

220 generated; Table 4 categorizes these metrics by type (for a full list of metrics included in the database, see
 221 Supplement A).

222 **Table 4. Types of point cloud metrics calculated from non-ground returns from ALS transects. In total, 369 metrics were**
 223 **generated. Metrics were calculated for four groups of returns using: (1) all returns above 0 m, (2) first returns above 0 m,**
 224 **(3) all returns above 2 m, and (4) first returns above 2 m. For a full list of metrics see Supplement A, and for detailed**
 225 **descriptions see Tompalski (2024).**

Metric types	Description	Example metrics
Simple descriptive statistics	Basic statistical measures (e.g., mean, variance, skewness) summarizing point cloud height distribution (Bouvier et al., 2015; Lefsky et al., 2005; Nilsson, 1996).	zmean zsd_above2
Number of points by return number	Counts of ALS returns classified by return order.	n_return_1 n_return_4_above2
Number and proportion of returns by echo type	The count and relative frequency of returns categorized as single, first, intermediate, or last echoes.	n_last n_intermediate_above2
Height percentiles	Specific quantiles (e.g., 10th, 50th, 90th percentile) of the point cloud height distribution.	zq5 zq50_above2_first
Proportion of returns above threshold height	The fraction of returns exceeding a predefined height, used to characterize canopy cover (Solberg et al., 2006).	pzabove2 pzabovemean_first
Vertical structure	Metrics describing the distribution and variation of ALS returns along the vertical axis (van Ewijk et al., 2011; Shannon, 1948).	ziqr VCI_above2_first
Cumulative point density	The cumulative proportion of returns found in nine equal height intervals (Woods et al., 2008).	zpcum1 zpcum5_above2_first
L-moments metrics	Statistical measures capturing the shape of the height distribution, providing robust alternatives to conventional descriptive statistics (Frazer et al., 2011).	Lcoefvar L1_above2
Metrics based on leaf area density	Estimates of foliage distribution and density (Hopkinson et al., 2013; Magnussen and Boudewyn, 1998).	lad_mean lad_min_above2
Interval metrics	Metrics derived from predefined height intervals, summarizing point density at different canopy levels.	pz_1_2 pz_8_9_first
Rumple	A measure of canopy surface roughness or complexity based on the ratio of 3D to 2D surface area (Kane et al., 2010).	rumple rumple_above2_first
Metrics based on kernel density estimation	Metrics derived from smoothed height distributions (McGaughey, 2024).	kde_peak3_elev kde_peak2_diff_above2_first

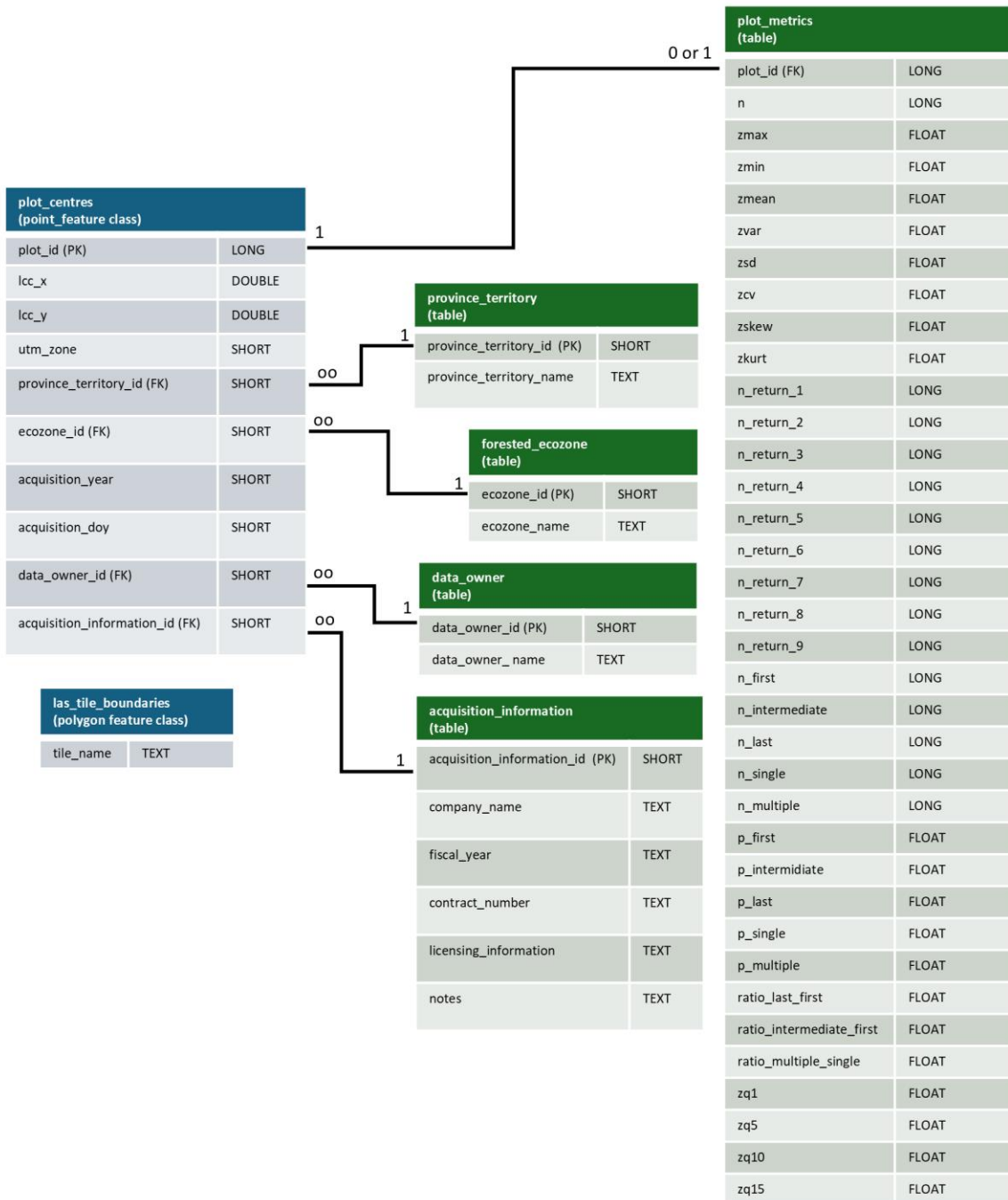
226

227 **2.4 Lidar plots database**

228 Lidar plots and associated point cloud metrics are distributed as SQLite GeoPackages¹, which are an open and non-
229 proprietary format. Each acquisition year (i.e., 2023, 2024, and 2025) will be stored in a separate database. Each
230 GeoPackage contains a point feature class storing lidar plots on the NTEMS 30 m grid, a feature class delineating
231 point cloud footprints, as well as a series of data tables storing point cloud metrics, province or territory, UTM zone,
232 ecozone, and information related to individual acquisitions (Figure 2). Given the large number of metrics in the full
233 database (Supplement A), for each year an abridged version of the dataset is also being shared that contains a subset
234 of commonly used metrics for forest inventory (White et al., 2013, 2017a; Supplement B).

235

¹ <https://www.geopackage.org/>



Note: too many fields to list

236

237
238
239

Figure 2. Entity relationship diagram describing the structure of the lidar plots database. In total, the plot metrics table includes 369 point cloud metrics for each lidar plot, with an abridged version of the database available including a subset of 40 metrics.

240 3 Results

241 3.1 ALS transects acquisitions

242 A total of ~20,000 km² ~~and~~ ~23,000 km² ~~and~~ ~12,000 km² of ALS transect data were acquired in 2023, ~~and~~ 2024,
243 ~~and 2025~~, respectively (Figure 1). The 2023 acquisition focused on collecting data over forest-dominated ecozones
244 that are currently lacking ALS coverage (White et al., 2025). The 2023 ALS acquisitions were significantly impacted
245 by smoke caused by unprecedented wildfire activity in Canada (Jain et al., 2024), and as a result, 5,000 km of
246 planned acquisitions were postponed for capture in 2024. The 2024 ~~and 2025~~ transects focused on acquiring data
247 over NorthForM ground plots (Boucher et al., 2023). ~~In 2025, wildfire activity and inclement weather resulted in~~
248 ~~only 64% of planned data acquired. ~~with~~ During the 2023, 2024, and 2025 field seasons over 900 ground ~~~650~~~~
249 plots ~~were captured~~ measured. Table 5 summarizes sampling intensity within NTEMS treed land cover classes ~~for the~~
250 ~~2023 acquisition~~ (Hermosilla et al., 2022) by ecozone (Figure 1).

251

252 **Table 5. Sampling intensity within treed land cover classes by ecozone for 2023. “Land cover pixel area (ha)” represents**
 253 **the area classified as a given land cover type within the ecozone (Figure 1). “Land cover pixel area (%)“ is the percent**
 254 **coverage of a given land cover type in an ecozone. “Lidar plot area (ha)” represents the area of lidar plots within the**
 255 **ecozone that falls within a given land cover type. “Sampling intensity (%)” is calculated as lidar plot area divided by pixel**
 256 **area and multiplied by 100.**

Ecozone	Land cover class	Land cover pixel area (ha)	Land cover pixel area (%)	Lidar plot area (ha)	Sampling intensity (%)
Boreal Cordillera	Wetland-treed	656,907	1.5	2,609	0.3972
	Coniferous	21,292,772	47.9	79,718	0.3744
	Broadleaf	1,286,953	2.9	2,915	0.2265
	Mixedwood	729,463	1.6	1,113	0.1526
Boreal Plains	Wetland-treed	5,732,402	8.0	7,930	0.1383
	Coniferous	17,817,472	25.0	15,142	0.0850
	Broadleaf	13,063,662	18.3	5,860	0.0449
	Mixedwood	2,104,651	2.9	2,437	0.1158
Boreal Shield East	Wetland-treed	1,787,152	1.4	4,888	0.2735
	Coniferous	42,287,435	34.2	99,850	0.2361
	Broadleaf	8,328,982	6.7	2,115	0.0254
	Mixedwood	23,206,039	18.8	23,272	0.1003
Boreal Shield West	Wetland-treed	3,803,299	4.6	35,432	0.9316
	Coniferous	24,556,792	30.0	209,945	0.8549
	Broadleaf	2,946,598	3.6	8,100	0.2749
	Mixedwood	18,467,937	22.5	90,821	0.4918
Hudson Plains	Wetland-treed	13,322,381	30.6	27,665	0.2077
	Coniferous	2,970,087	6.8	10,084	0.3395
	Broadleaf	112,246	0.3	396	0.3526
	Mixedwood	1,107,734	2.5	5,939	0.5362
Taiga Plains	Wetland-treed	2,291,152	3.7	30,805	1.3445
	Coniferous	24,969,142	40.3	163,272	0.6539
	Broadleaf	2,721,976	4.4	28,823	1.0589
	Mixedwood	886,926	1.4	5,993	0.6757
Taiga Shield East	Wetland-treed	210,365	0.3	1	0.0005
	Coniferous	28,408,741	36.0	6,259	0.0220
	Broadleaf	192,614	0.2	1	0.0005
	Mixedwood	493,404	0.6	6	0.0012
Taiga Shield West	Wetland-treed	361,229	0.6	237	0.0656
	Coniferous	17,872,110	29.9	45,534	0.2548
	Broadleaf	865,552	1.4	1,441	0.1664
	Mixedwood	741,346	1.2	853	0.1151

257

258 **3.1.2 Quality assurance results**

259 Overall, the ALS acquisition specifications (Table 1) were met and often exceeded. A rare exception, however, were
260 periodic changes in footprint sizes, swath widths, and point densities in areas with complex topography. These
261 deviations are not unexpected and occur mostly in the mountainous areas of western Canada above the tree line, and
262 impact less than one percent of the transect data.

263 The ALS vendors (Table 2) corrected GNSS coordinates using PPP, with all reporting sub-metre horizontal and
264 vertical accuracies. Point cloud classifications were validated following guidance in section 8.6 of the Canadian lidar
265 acquisition standards (CSA Group, 2025), which indicate that point classifications should be consistent across the
266 entire project with minimal variations in the classification quality between tiles or swaths. For each acquisition year,
267 twenty 1 km x 1 km point cloud tiles distributed across the acquisition areas (Figure 1) were selected for analysis.
268 Within each tile, 20 randomly selected 400 m² areas were then clipped and three-dimensional visual checks of the
269 point cloud classifications were performed using FUSION's pdq viewer (McGaughey, 2024). All point clouds were
270 rasterized based on return class (Table 1) and hillshades were generated from the DTMs. Raster surfaces were then
271 visually inspected to ensure specifications were met (e.g., all points were classified (unless withheld), water was
272 properly classified, no areas with few or no ground returns, noise was classified correctly, DTMs were representative
273 of the bare-Earth surface). Similarly, return counts and scan angles were rasterized to ensure transects fell within the
274 specifications for point densities and swath widths (Table 1). All raster products were generated using LAStools
275 (version 2.0.4). Any issues found were reported to the ALS data vendors who then made corrections.

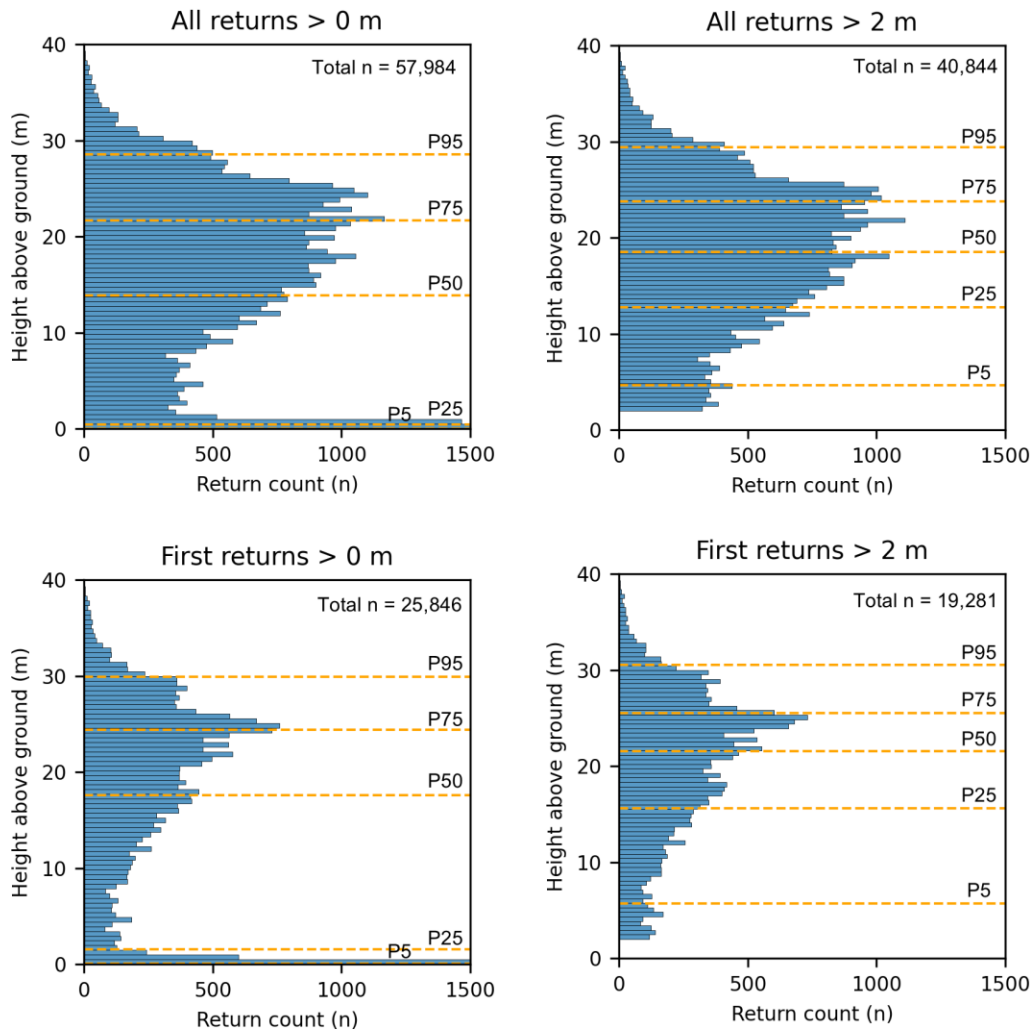
276 ~~The ALS vendors (Table 2) corrected GNSS data using PPP and all reported sub-metre horizontal and vertical~~
277 ~~accuracies. Areas where transects overlap tended to have vertical differences in their digital terrain models (DTM) of~~
278 ~~several decimetres. Point cloud classifications were validated using methods described in section 8.6 of the~~
279 ~~Canadian lidar acquisition standards (CSA Group, 2025) by randomly selecting 20 x 20²m areas that were then~~
280 ~~clipped to perform three-dimensional visual checks of the data. Point clouds were also rasterized based on return~~
281 ~~class (Table 1) and hillshades were generated from the DTMs. Raster surfaces were then visually inspected to ensure~~
282 ~~specifications were met (e.g., water was properly classified, DTMs were representative of the bare Earth surface).~~
283 ~~Similarly, return counts and scan angles were rasterized to ensure transects fell within the specifications for point~~
284 ~~densities and swath widths (Table 1). All raster products were generated using LAStools (version 2.0.4).~~

285 **3.2 Lidar plots databases**

286 For the 2023 ALS transects, 15,353,866 lidar plots were generated within the lidar swaths. The full database
287 including 369 point cloud metrics is 60.2 GB in size, and the abridged version of the database containing a subset of
288 40 metrics is 7.2 GB. Both versions are shared as SQLite GeoPackages.

289 **3.3 Point cloud metrics**

290 Point cloud metrics were processed in four groups using: (1) all returns above 0 m, (2) first returns above 0 m, (3) all
 291 returns above 2 m, and (4) first returns above 2 m. Figure 3 shows an example of the four processing groups from
 292 the same lidar plot. The number of returns range from 19,281 (first returns > 2m) to 57,984 (all returns > 0m), while
 293 the height percentiles change by varying degrees between each group. The lower height percentiles are most
 294 sensitive to changes in height threshold, with the first return P5 changing from 0.06 m (0 m threshold) to 5.71m (2 m
 295 threshold), while P95 changes from 29.91 m (0 m threshold) to 30.55 m (2 m threshold).



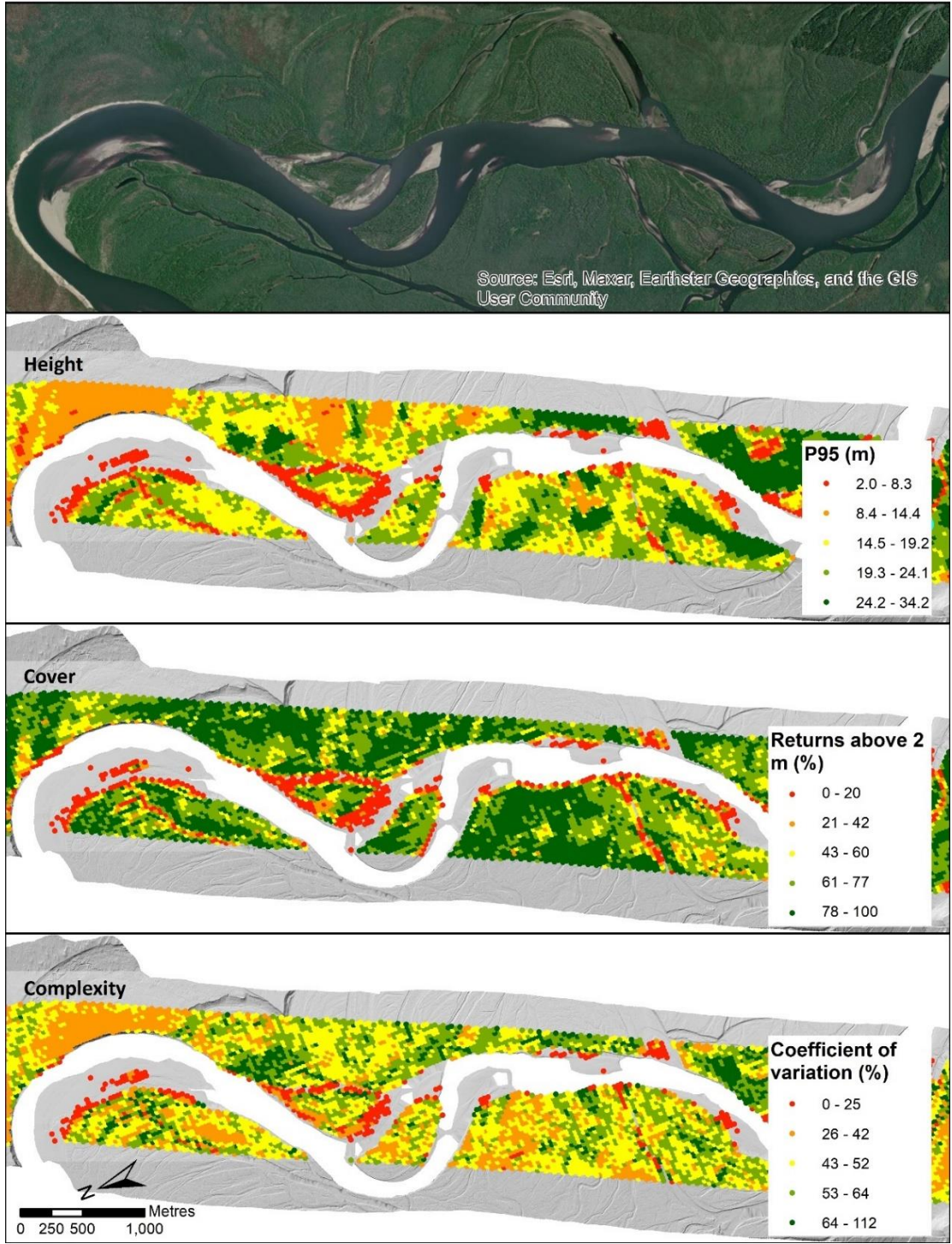
296

297 **Figure 3. Comparison of vertical distributions of returns from four different processing groups for the same lidar plot: all**
 298 **returns above 0 m, all returns above 2 m, first returns above 0 m, and first returns above 2 m. P95 = 95th height**
 299 **percentile, P75 = 75th height percentile, and so on. The plot is located along the Prophet River in northern British**
 300 **Columbia (58° 17' 19" N, 122° 52' 30" W).**

301

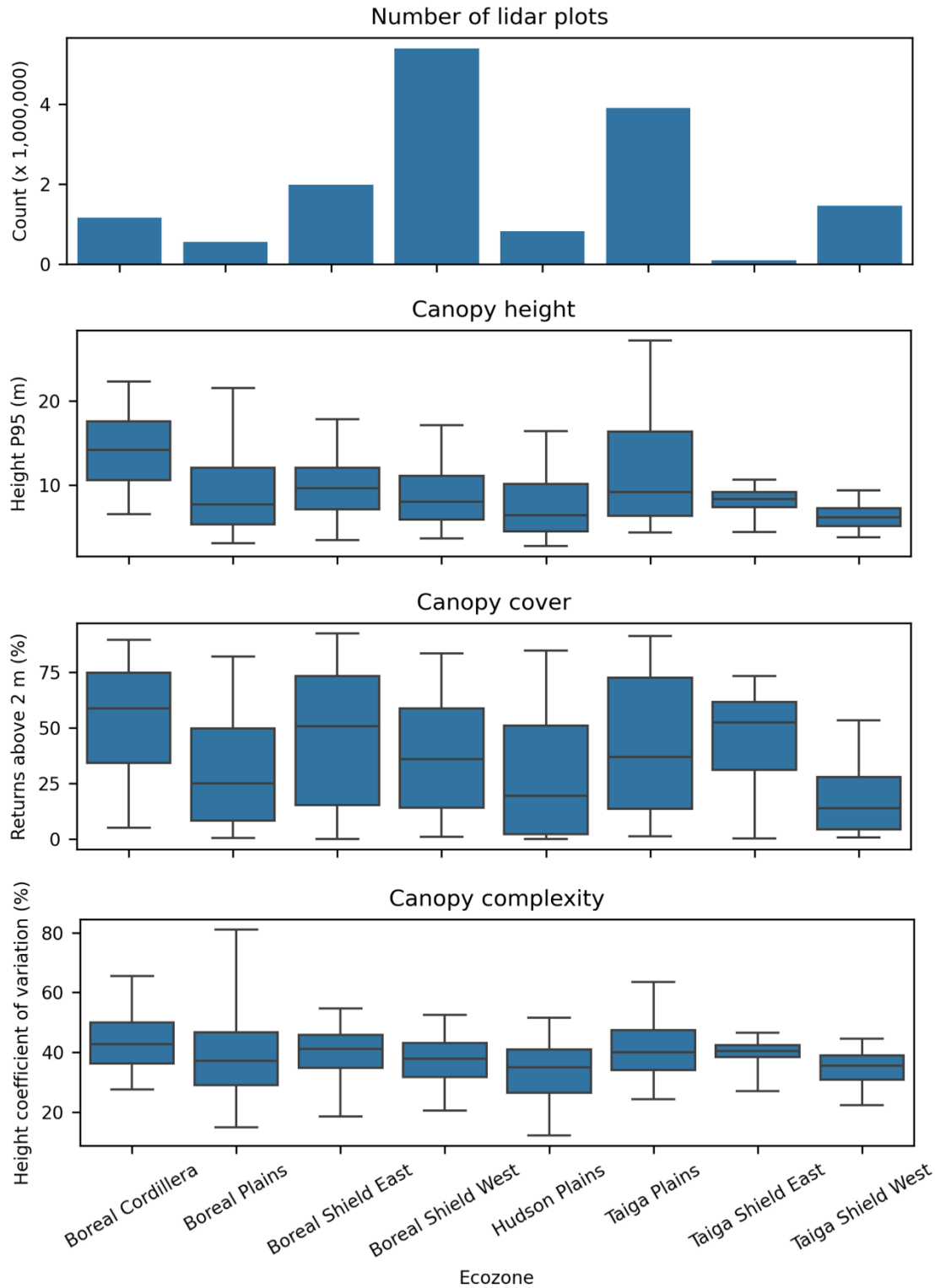
302 Fundamentally, lidar characterizes vegetation height, vertical structure, and cover (Li et al., 2008). Figure 4 shows
 303 examples of lidar plots with point cloud metrics related to these attributes along a reach of the Liard River in

304 Northern British Columbia. Figure 5 provides summaries of height, cover and structure by ecozone for all 2023 lidar
305 plots.
306



307

308 Figure 4. Examples of lidar plot metrics, including: canopy height based on the 95th height percentile of first returns
 309 greater than 2 m; canopy cover based on the proportion of first returns greater than 2 m; and canopy complexity based
 310 on the coefficient of variation of first returns heights greater than 2m. The image in the top panel extends beyond the ALS
 311 swath for added landscape context. The digital terrain model hillshade was derived from ALS returns with scan angles in
 312 excess of 20 degrees, while lidar plots are limited to returns with scan angles less than or equal to 20 degrees (Table 1).
 313 Data are located along the Liard River in northern British Columbia (59° 53' 22" N, 128° 19' 3" W).

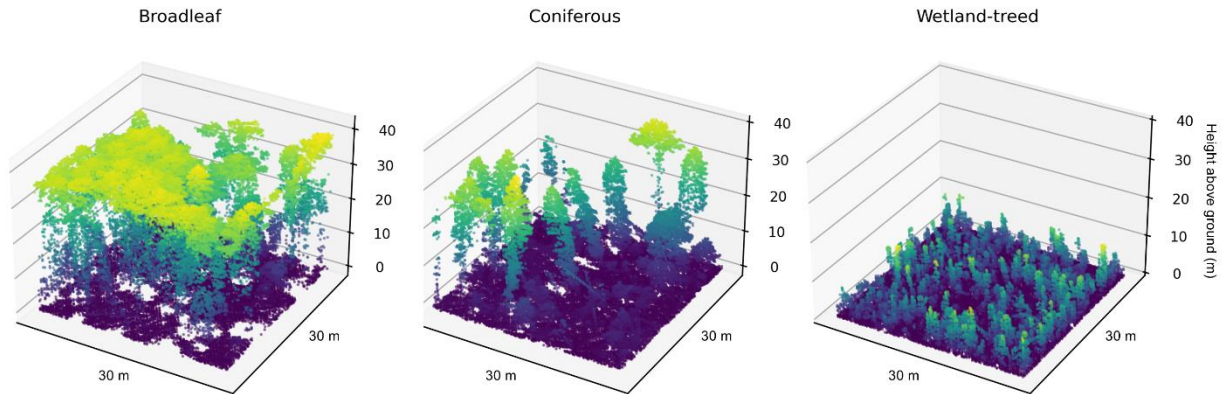


314

315 **Figure 5: Summary of vegetation metrics by ecozone (Figure 1) for the 2023 acquisition (total n = 15,353,866 lidar plots).**
 316 **For the box and whisker plots, the box represents the interquartile range with the centre line showing the median, while**
 317 **the whiskers represent the 5th and 95th percentiles.**

318 **3.3.1 Comparison of lidar plots with NTEMS satellite information products**

319 The NTEMS project provides a number of satellite-derived products characterizing forest-dominated ecozones,
320 including land cover (Hermosilla et al., 2022) and recent wildfire disturbance history (Hermosilla et al., 2016).
321 Figure 6 provides examples of point clouds clipped to lidar plots in three different treed land cover types. The
322 broadleaf and coniferous plots are located in productive riparian stands, while the wetland-treed plot is located in a
323 nearby treed bog or fen.

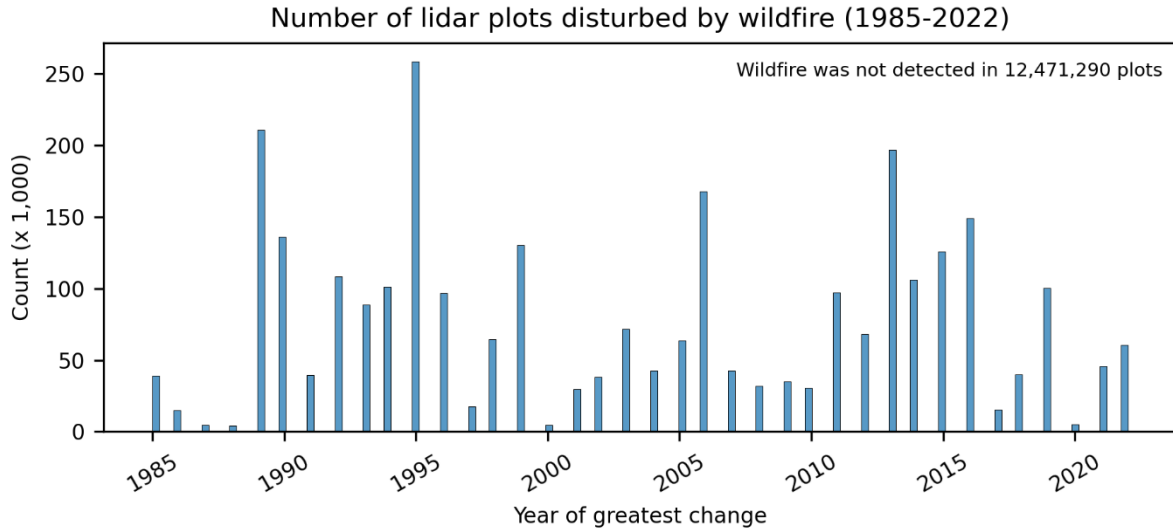
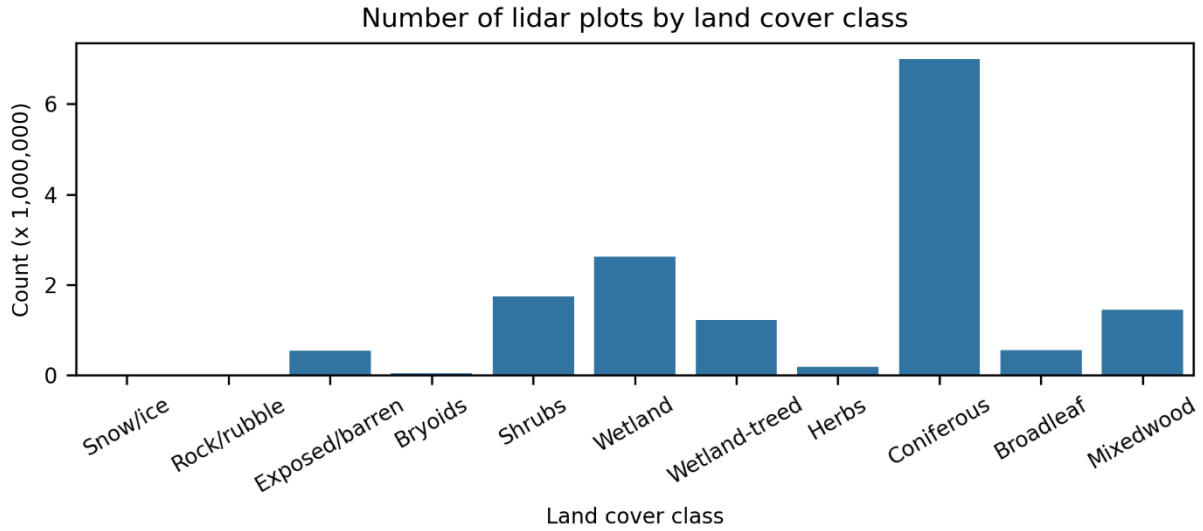


324
325 **Figure 6. Examples of point clouds within lidar plots for three different treed land cover types. The plots are located along**
326 **the Prophet River in northern British Columbia (58° 17' 19" N, 122° 52' 30" W).**

327
328 Figure 7 provides distributions of 2023 lidar plots for land cover and year of recent wildfire disturbance (1985 -
329 2022). For the 15,353,866 plots, the dominant land cover type (Hermosilla et al., 2022), excluding water within the
330 plots, was coniferous (46%), followed by wetland (17%), shrubs (11%), mixedwood (9%), wetland-treed (8%),
331 broadleaf (4%), exposed/barren land (3%), herbs (1%), bryoids (0.3%), rock/rubble (0.04%), and snow/ice
332 (0.001%). Moreover, 19% were disturbed by wildfire (Hermosilla et al., 2016) between 1985 and 2022 (Figure 7).

333

334



335

336

337

Figure 7. Comparison between lidar plots and multidecadal NTEMS satellite information products, including land cover class (excluding water) and number of plots disturbed by wildfire between 1985 and 2022 (Hermosilla et al., 2016; 2022).

338 4 Discussion

339 The ALS transects, lidar plots, and point cloud metrics presented here represent a comprehensive and coordinated
340 effort to sample forest structure in Canada's unmanaged northern forests. By collecting high-density ALS data
341 across ecologically diverse regions that lack structural information, this dataset fills a critical gap in the national
342 forest monitoring landscape. The design and implementation of the acquisitions can address both scientific and
343 operational needs, with particular relevance to wildfire fuel mapping (Andersen et al., 2005; Martin-Ducup et al.,
344 2025; Riaño et al., 2003), forest inventory (Reutebuch et al., 2005; Wulder et al., 2008), carbon accounting
345 (Andersen et al., 2011; Babcock et al., 2018), and ecosystem monitoring (Bolton et al., 2015; Matasci et al., 2018b).

346 Open datasets allow fire researchers and other specialists unfamiliar with ALS point cloud processing to access these
347 data in an analysis-ready and easy-to-use format. We chose to package the data as SQLite GeoPacackages, using
348 vector feature classes to store spatial data. The aim is to ensure that the data ~~are readily~~ are readily accessible and
349 easy to use for those familiar with geographic information systems or scientific programming languages such as
350 Python, R or Julia. While ALS derivatives are typically distributed using raster formats (e.g. Assmann et al., 2022;
351 Shi et al., 2025), the layout of the transects (Figure 1) would result in raster surfaces consisting largely of "no data"
352 values. Should a user desire, the point feature classes can be easily rasterized for inclusion in an analysis workflow
353 requiring gridded surfaces. For users interested in leveraging NTEMS datasets (e.g. Hermosilla et al., 2022, 2024;
354 Matasci et al., 2018a, b), the lidar plots will integrate seamlessly as all data share a common spatial resolution,
355 projection (Table 3), and origin coordinates. Should users prefer to generate metrics at other spatial resolutions, the
356 raw ALS point cloud data will also be made publicly available.

357 A key advantage of this dataset lies in its flexibility. The inclusion of point cloud metrics from the four combinations
358 of return types and height thresholds (all returns and first returns, > 0 m and > 2 m) supports diverse modeling
359 approaches, including forest inventory, regeneration assessment, and canopy fuel characterization (Table 4, Figure 3,
360 Supplement A, Supplement B). For those focused on developing forest inventories, point cloud metrics based on
361 returns above 2 m, which remove the effects of shrubs and small trees, may be the most appropriate. For users
362 interested in forest regeneration or fuels attributes such as canopy base height, retaining lower returns may be
363 beneficial (Arumäe and Lang, 2018; Naesset, 2011; Stefanidou et al., 2020). The decision to use first returns or all
364 returns may be guided by examining performance diagnostics from predictive models (Arumäe and Lang, 2018;
365 Bater et al., 2011). White et al. (2013, 2017a) provide advice on model development for enhanced forest inventories,
366 and the methods described and citations therein can inform a wide range of applications related to ALS and ecology.

367 The value of lidar plots lies in their role as a scalable intermediary between field measurements and satellite-based
368 inventories, effectively increasing the sample size of required model inputs (Wulder et al. 2012b). When integrated
369 with ground plots and satellite data, lidar plots can enable the generation of wall-to-wall maps of forest attributes
370 such as height, volume, and biomass. This approach has been demonstrated nationally for Canada's forests using
371 previously acquired ALS transects (Matasci et al., 2018a, b) and the expansion of this sampling framework with the
372 new acquisitions described herein substantially increases coverage across previously unsampled areas.

373 Despite the aforementioned strengths of lidar plots, several aspects of these data warrant further consideration. In
374 particular, the ALS acquisitions are largely restricted to northern forests (Figure 1). Given the focused sampling to
375 these northern forests, conditions present in the southern extent of Canada’s forests will not be captured, as
376 exemplified by the distributions of land cover classes within lidar plots (Figure 7), which differ markedly from the
377 national summaries reported by Hermosilla et al. (2022). As these lidar transects were specifically designed to
378 characterize northern forest conditions, they would need to be augmented with ALS data from southern forests to
379 enable the development of national models of forest structure, as demonstrated in Matasci et al. (2018b). With more
380 than 70% of Canada’s managed forest area in the south having ALS data available (White et al., 2025), additional
381 samples of ALS are readily available. Sampled transects also inhabit an unfamiliar form and scale for most users of
382 ALS data. Within the lidar plots can be found detailed characterizations of both vegetation structure and terrain
383 morphology (Figure 4, Figure 6). The data can also be analyzed at regional scales, by pooling lidar plots (Figure 5)
384 to contribute to population estimates of attributes such as volume or biomass (Andersen et al., 2011; Margolis et al.,
385 2015). However, by design transect data alone are not spatially exhaustive, precluding independent wall-to-wall
386 mapping, and are intended to be incorporated with satellite and other ancillary data to support mapping via
387 modelling methods such as imputation (Coops et al., 2021).

388 ~~Despite these strengths, several aspects warrant consideration. In particular, the ALS acquisitions are restricted to~~
389 ~~northern forests. Given the focused sampling to these northern forests, conditions present in the south will not be~~
390 ~~captured, as exemplified by the distributions of land cover classes within lidar plots (Figure 7) differing markedly~~
391 ~~from the national summaries reported by Hermosilla et al. (2022). These differences point to limitations of the~~
392 ~~transects for developing national predictive models of forest structure, with a need to obtain additional samples to~~
393 ~~represent managed forests via partnerships with provincial agencies or other accessible sources of ALS data (White~~
394 ~~et al., 2025). Sampled transects also inhabit an unfamiliar form and scale for most users of ALS data. Within the~~
395 ~~transects can be found detailed characterizations of both vegetation structure and terrain morphology (Figure 4,~~
396 ~~Figure 6). The data can also be analyzed at regional scales (Figure 5) to contribute to population estimates of~~
397 ~~attributes such as volume or biomass (Andersen et al., 2011; Margolis et al., 2015). However, transect data alone are~~
398 ~~not spatially exhaustive, precluding independent wall to wall mapping and requiring the incorporation of satellite or~~
399 ~~other ancillary data and modelling methods such as imputation (Coops et al., 2021).~~

400 One of the objectives of the NorthForM program is the collection of coincident ALS and ground plot data. As the
401 program progresses, GNSS locations from ground plots will be used to clip ALS point clouds to the plot extents. The
402 same suite of 369 metrics described above (Table 4, Supplement A) will then be generated for the ground plots and
403 made available. In combination, the forest inventory measurements made in situ within ground plots, ground plot
404 point cloud metrics, and the lidar plot point cloud metrics will be powerful datasets for the spatially explicit
405 predictive modelling of forest structure (Matasci et al., 2018a, b; Zald et al., 2016).

407 These data will be used for a number of initiatives. Wildfire specialists will employ the data to contribute to the
408 development of predictive models that estimate fuel attributes such as canopy species composition, crown base
409 height, crown bulk density, forest floor cover type, and litter load (Boucher et al., 2023). National models of forest
410 inventory attributes will be improved and brought up-to-date, including those related to height, structural
411 complexity, biomass, and volume (Matasci et al., 2018b). The data will also inform carbon accounting by
412 contributing to the development of pixel-based biomass yield curves (Tompalski et al., 2025).

413 Beyond Canada, the ALS transect network provides an example for characterizing vegetation structure over large
414 areas at a relatively low cost. The transects-based approach offers a transferable framework for designing national
415 forest monitoring programs in countries where consistent, high spatial resolution structural data are lacking. By
416 linking ALS measurements to ground plots and satellite observations, the dataset can support regional to global
417 assessments of carbon stocks, disturbance dynamics, and climate-driven change.

418 Herein we focus largely on point cloud metrics derived from ALS data acquired in 2023; however, data collected in
419 2024 and 2025 will be made available following the same processing stream and use the same basic database
420 schema described herein. The addition of terrain metrics (e.g. height, slope, curvature, solar radiation) is underway
421 and will be included as an additional table in future releases. The raw ALS point cloud data will also be made
422 publicly available.

423 **5 Data availability**

424 The 2023 lidar plots and point cloud metrics described here are available at
425 <https://doi.org/10.5281/zenodo.16782860> on Zenodo (Bater et al., 2025).

426 The 2023 data and collections from subsequent acquisition years collected under the same monitoring framework
427 will be released as independent datasets and will share a common structure and repository. They will be made
428 available through Canada's National Forest Information System (NFIS) at: [https://opendata.nfis.org/mapserver/nfis-](https://opendata.nfis.org/mapserver/nfis-change_eng.html)
429 [change_eng.html](https://opendata.nfis.org/mapserver/nfis-change_eng.html)

430 The most current versions of the metrics databases and raw ALS point clouds will be made findable through NFIS.

431 **6 Conclusion**

432 The lidar plots and point cloud metrics described herein form part of an open-data initiative to enhance structural
433 information on Canada's northern forests. By sampling remote and underrepresented forest-dominated ecozones,
434 this dataset supports key applications in wildfire risk assessment, forest inventory, and ecosystem monitoring. These
435 data offer a scalable foundation for integrating field and satellite observations to inform national mapping and
436 monitoring efforts, helping address long-standing data gaps in Canada's forest information landscape. In
437 combination with similar lidar plots representing conditions in southern Canada, these data form a key input towards
438 updating and improving the structural data layers (e.g., biomass, canopy height and cover) delivered via the National

439 Terrestrial Ecosystem Monitoring System. The inclusion of a wide range of metrics provides flexibility for diverse
440 predictive modeling needs, while the database structure ensures usability by researchers and practitioners who may
441 not be well-versed in remote sensing.

442 **Author contribution**

443 Conceptualization by MW, JW, TH, and CB. Data curation by CB. Formal analysis by CB. Methodology by JW, CB,
444 HC, and PT. Software by CB, HC, and PT. Supervision by MW, JW, and TH. Writing by CB, MW, JW, TH, and PT..

445 **Competing interests**

446 The contact author has declared that neither they nor their co-authors have any competing interests.

447 **Acknowledgements**

448 The ALS data were acquired with funding from the Canadian Forest Service's Northern Forest Mapping
449 (NorthForM) program, which aims to enhance mapping of Canada's northern forests, identify wildfire hazards, and
450 support community wildfire resilience and mitigation measures.

451 We thank Jonathan Boucher (Canadian Forest Service, Laurentian Forestry Centre) for his invaluable insights into
452 the next generation of the Canadian Forest Fire Danger Rating System and how remote sensing data can support
453 future fire behaviour models.

454 **References**

455 Aldred, A. and Bonnor, G. M.: Application of airborne lasers to forest surveys, Canadian Forestry Service,
456 Petawawa National Forestry Centre. 62p, 1985.

457 Andersen, H. E., McGaughey, R. J., and Reutebuch, S. E.: Estimating forest canopy fuel parameters using LIDAR
458 data, *Remote Sens. Environ.*, 94, 441–449, <https://doi.org/10.1016/j.rse.2004.10.013>, 2005.

459 Andersen, H. E., Strunk, J., and Temesgen, H.: Using airborne light detection and ranging as a sampling tool for
460 estimating forest biomass resources in the upper Tanana Valley of interior Alaska, *West. J. Appl. For.*, 26, 157–164,
461 <https://doi.org/10.1093/wjaf/26.4.157>, 2011.

462 Arumäe, T. and Lang, M.: Estimation of canopy cover in dense mixed-species forests using airborne lidar data, *Eur.*
463 *J. Remote Sens.*, 51, 132–141, <https://doi.org/10.1080/22797254.2017.1411169>, 2018.

464 Assmann, J. J., Moeslund, J. E., Treier, U. A., and Normand, S.: EcoDes-DK15: High-resolution ecological
465 descriptors of vegetation and terrain derived from Denmark's national airborne laser scanning data set, *Earth Syst.*
466 *Sci. Data*, 14, 823–844, <https://doi.org/10.5194/essd-14-823-2022>, 2022.

467 Babcock, C., Finley, A. O., Andersen, H. E., Pattison, R., Cook, B. D., Morton, D. C., Alonzo, M., Nelson, R.,

468 Gregoire, T., Ene, L., Gobakken, T., and Næsset, E.: Geostatistical estimation of forest biomass in interior Alaska
469 combining Landsat-derived tree cover, sampled airborne lidar and field observations, *Remote Sens. Environ.*, 212,
470 212–230, <https://doi.org/10.1016/j.rse.2018.04.044>, 2018.

471 Bater, C., White, J., Chen, H., Tompalski, P., Hermosilla, T., and Wulder, M.: Lidar plots and point cloud metrics
472 derived from airborne laser scanning transects acquired over forests in northern Canada., *Zenodo*,
473 <https://doi.org/10.5281/zenodo.16782860>, 2025.

474 Bater, C. W., Wulder, M. A., Coops, N. C., Nelson, R. F., Hilker, T., and Nasset, E.: Stability of sample-based
475 scanning-LiDAR-derived vegetation metrics for forest monitoring, *IEEE Trans. Geosci. Remote Sens.*, 49, 2385–
476 2392, <https://doi.org/10.1109/TGRS.2010.2099232>, 2011.

477 Bolton, D. K., Coops, N. C., and Wulder, M. A.: Characterizing residual structure and forest recovery following
478 high-severity fire in the western boreal of Canada using Landsat time-series and airborne lidar data, *Remote Sens.*
479 *Environ.*, 163, 48–60, <https://doi.org/10.1016/j.rse.2015.03.004>, 2015.

480 Boucher, J., Cotton-Gagnon, A., Zerb, J., Smiley, B. P., Russo, G., and Nolan, M.: Field guide: sampling fuels in the
481 context of the Next-Generation Canadian Forest Fire Danger Rating System (NG-CFFDRS). *Field Sampling*
482 *Protocol and List of Attributes for Field Crews (2023)*, 26 pp., 2023.

483 Bourdeau-Goulet, S. and Hassanzadeh, E.: Comparisons between CMIP5 and CMIP6 models: simulations of climate
484 indices influencing food security, infrastructure resilience, and human health in Canada, *Earth’s Futur.*, 9,
485 e2021EF001995, <https://doi.org/https://doi.org/10.1029/2021EF001995>, 2021.

486 Bouvier, M., Durrieu, S., Fournier, R. A., and Renaud, J. P.: Generalizing predictive models of forest inventory
487 attributes using an area-based approach with airborne LiDAR data, *Remote Sens. Environ.*, 156, 322–334,
488 <https://doi.org/10.1016/j.rse.2014.10.004>, 2015.

489 Brandt, J. P.: The extent of the North American boreal zone, *Environ. Rev.*, 17, 101–161,
490 <https://doi.org/10.1139/A09-004>, 2009.

491 Burton, P. J.: Understanding spring wildfires in Canada’s northern forests, *Glob. Chang. Biol.*, 29, 5983–5985,
492 <https://doi.org/10.1111/gcb.16879>, 2023.

493 Canadian Forest Service Fire Danger Group: An overview of the next generation of the Canadian Forest Fire Danger
494 Rating System (Information Report GLC-X-26)., 70 pp., 2021.

495 Coops, N. C., Tompalski, P., Goodbody, T. R. H., Queinnec, M., Luther, J. E., Bolton, D. K., White, J. C., Wulder,
496 M. A., van Lier, O. R., and Hermosilla, T.: Modelling lidar-derived estimates of forest attributes over space and
497 time: A review of approaches and future trends, *Remote Sens. Environ.*, 260, 112477,
498 <https://doi.org/10.1016/j.rse.2021.112477>, 2021.

499 Crowley, M. A., Stockdale, C. A., Johnston, J. M., Wulder, M. A., Liu, T., McCarty, J. L., Rieb, J. T., Cardille, J.

500 A., and White, J. C.: Towards a whole-system framework for wildfire monitoring using Earth observations, *Glob.*
501 *Chang. Biol.*, 29, 1423–1436, <https://doi.org/10.1111/gcb.16567>, 2023.

502 CSA Group: Airborne lidar data acquisition, 83 pp., <https://www.csagroup.org/store/product/2431645/>, 2025.

503 van Ewijk, K. Y., Treitz, P. M., and Scott, N. A.: Characterizing forest succession in central Ontario using lidar-
504 derived indices, *Photogramm. Eng. Remote Sensing*, 77, 261–269, <https://doi.org/0099-1112>.
505 DOI:10.1117/12.2223586, 2011.

506 Fassnacht, F. E., White, J. C., Wulder, M. A., and Næsset, E.: Remote sensing in forestry: current challenges,
507 considerations and directions, *For. An Int. J. For. Res.*, 97, 11–37, <https://doi.org/10.1093/forestry/cpad024>, 2024.

508 Frazer, G. W., Magnussen, S., Wulder, M. A., and Niemann, K. O.: Simulated impact of sample plot size and co-
509 registration error on the accuracy and uncertainty of LiDAR-derived estimates of forest stand biomass, *Remote*
510 *Sens. Environ.*, 115, 636–649, <https://doi.org/10.1016/j.rse.2010.10.008>, 2011.

511 Gillis, M. D., Omule, A. Y., and Brierley, T.: Monitoring Canada’s forests: The National Forest Inventory, *For.*
512 *Chron.*, 81, 214–221, <https://doi.org/10.5558/tfc81214-2>, 2005.

513 Guindon, L., Manka, F., Correia, D. L. P., Villemaire, P., Smiley, B., Bernier, P., Gauthier, S., Beaudoin, A.,
514 Boucher, J., and Boulanger, Y.: A new approach for Spatializing the CANadian National Forest Inventory (SCANFI)
515 using Landsat dense time series, *Can. J. For. Res.*, 2010, <https://doi.org/10.1139/cjfr-2023-0118>, 2024.

516 Hansen, M. C., Egorov, A., Potapov, P. V., Stehman, S. V., Tyukavina, A., Turubanova, S. A., Roy, D. P., Goetz, S.
517 J., Loveland, T. R., Ju, J., Kommareddy, A., Kovalskyy, V., Forsyth, C., and Bents, T.: Monitoring conterminous
518 United States (CONUS) land cover change with Web-Enabled Landsat Data (WELD), *Remote Sens. Environ.*, 140,
519 466–484, <https://doi.org/10.1016/j.rse.2013.08.014>, 2014.

520 Haslem, A., Kelly, L. T., Nimmo, D. G., Watson, S. J., Kenny, S. A., Taylor, R. S., Avitabile, S. C., Callister, K. E.,
521 Spence-Bailey, L. M., Clarke, M. F., and Bennett, A. F.: Habitat or fuel? Implications of long-term, post-fire
522 dynamics for the development of key resources for fauna and fire, *J. Appl. Ecol.*, 48, 247–256,
523 <https://doi.org/10.1111/j.1365-2664.2010.01906.x>, 2011.

524 Hermosilla, T., Wulder, M. A., White, J. C., Coops, N. C., Hobart, G. W., and Campbell, L. B.: Mass data
525 processing of time series Landsat imagery: pixels to data products for forest monitoring, *Int. J. Digit. Earth*, 9, 1035–
526 1054, <https://doi.org/10.1080/17538947.2016.1187673>, 2016.

527 Hermosilla, T., Wulder, M. A., White, J. C., and Coops, N. C.: Land cover classification in an era of big and open
528 data: Optimizing localized implementation and training data selection to improve mapping outcomes, *Remote Sens.*
529 *Environ.*, 268, 112780, <https://doi.org/10.1016/j.rse.2021.112780>, 2022.

530 Hermosilla, T., Wulder, M. A., White, J. C., Coops, N. C., Bater, C. W., and Hobart, G. W.: Characterizing long-
531 term tree species dynamics in Canada’s forested ecosystems using annual time series remote sensing data, *For. Ecol.*

532 Manage., 572, 122313, <https://doi.org/10.1016/j.foreco.2024.122313>, 2024.

533 Hopkinson, C., Wulder, M. A., Coops, N. C., Milne, T., Fox, A., and Bater, C. W.: Airborne lidar sampling of the
534 Canadian boreal forest: planning, execution, and initial processing., in: Proceedings of the SilviLaser 2011
535 Conference, 2011.

536 Hopkinson, C., Lovell, J., Chasmer, L., Jupp, D., Kljun, N., and van Gersel, E.: Integrating terrestrial and airborne
537 lidar to calibrate a 3D canopy model of effective leaf area index, *Remote Sens. Environ.*, 136, 301–314,
538 <https://doi.org/10.1016/j.rse.2013.05.012>, 2013.

539 Jain, P., Barber, Q. E., Taylor, S. W., Whitman, E., Castellanos Acuna, D., Boulanger, Y., Chavardès, R. D., Chen,
540 J., Englefield, P., Flannigan, M., Girardin, M. P., Hanes, C. C., Little, J., Morrison, K., Skakun, R. S., Thompson, D.
541 K., Wang, X., and Parisien, M.: Drivers and impacts of the record-breaking 2023 wildfire season in Canada, *Nat.*
542 *Commun.*, 15, 6764, <https://doi.org/10.1038/s41467-024-51154-7>, 2024.

543 Kane, V. R., Bakker, J. D., McGaughey, R. J., Lutz, J. A., Gersonde, R. F., and Franklin, J. F.: Examining conifer
544 canopy structural complexity across forest ages and elevations with LiDAR data, *Can. J. For. Res.*, 40, 774–787,
545 <https://doi.org/http://www.nrcresearchpress.com/doi/abs/10.1139/X10-064>, 2010.

546 Keane, R. E., Reinhardt, E. D., Scott, J., Gray, K., and Reardon, J.: Estimating forest canopy bulk density using six
547 indirect methods, *Can. J. For. Res.*, 35, 724–739, <https://doi.org/10.1139/x04-213>, 2005.

548 Keith, H., Mackey, B. G., and Lindenmayer, D. B.: Re-evaluation of forest biomass carbon stocks and lessons from
549 the world’s most carbon-dense forests, *Proc. Natl. Acad. Sci.*, 106, 11635–11640,
550 <https://doi.org/https://doi.org/10.1073/pnas.090197010>, 2009.

551 Lefsky, M. A., Cohen, W. B., Parker, G. G., and Harding, D. J.: Lidar remote sensing for ecosystem studies,
552 *Bioscience*, 52, 19–30, [https://doi.org/10.1641/0006-3568\(2002\)052\[0019:LRSFES\]2.0.CO;2](https://doi.org/10.1641/0006-3568(2002)052[0019:LRSFES]2.0.CO;2), 2002.

553 Lefsky, M. A., Hudak, A. T., Cohen, W. B., and Acker, S. A.: Patterns of covariance between forest stand and
554 canopy structure in the Pacific Northwest, *Remote Sens. Environ.*, 95, 517–531,
555 <https://doi.org/10.1016/j.rse.2005.01.004>, 2005.

556 Li, Y., Andersen, H., and McGaughey, R.: A comparison of statistical methods for estimating forest biomass from
557 light detection and ranging data, *West. J. Appl. For.*, 23, 223–231,
558 <https://doi.org/https://doi.org/10.1093/wjaf/23.4.223>, 2008.

559 Magnussen, S. and Boudewyn, P.: Derivations of stand heights from airborne laser scanner data with canopy-based
560 quantile estimators, *Can. J. For. Res.*, 28, 1016–1031, 1998.

561 Margolis, H. A., Nelson, R. F., Montesano, P. M., Beaudoin, A., Sun, G., Andersen, H. E., and Wulder, M. A.:
562 Combining satellite lidar, airborne lidar, and ground plots to estimate the amount and distribution of aboveground
563 biomass in the boreal forest of North America, *Can. J. For. Res.*, 45, 838–855, <https://doi.org/10.1139/cjfr-2015->

564 0006, 2015.

565 Martin-Ducup, O., Dupuy, J. L., Soma, M., Guerra-Hernandez, J., Marino, E., Fernandes, P. M., Just, A., Corbera,
566 J., Toutchkov, M., Sorribas, C., Bock, J., Piboule, A., Pirotti, F., and Pimont, F.: Unlocking the potential of Airborne
567 LiDAR for direct assessment of fuel bulk density and load distributions for wildfire hazard mapping, *Agric. For.
568 Meteorol.*, 362, <https://doi.org/10.1016/j.agrformet.2024.110341>, 2025.

569 Matasci, G., Hermosilla, T., Wulder, M. A., White, J. C., Coops, N. C., Hobart, G. W., and Zald, H. S. J.: Large-area
570 mapping of Canadian boreal forest cover, height, biomass and other structural attributes using Landsat composites
571 and lidar plots, *Remote Sens. Environ.*, 209, 90–106, <https://doi.org/10.1016/j.rse.2017.12.020>, 2018a.

572 Matasci, G., Hermosilla, T., Wulder, M. A., White, J. C., Coops, N. C., Hobart, G. W., Bolton, D. K., Tompalski, P.,
573 and Bater, C. W.: Three decades of forest structural dynamics over Canada’s forested ecosystems using Landsat
574 time-series and lidar plots, *Remote Sens. Environ.*, 216, 697–714, <https://doi.org/10.1016/j.rse.2018.07.024>, 2018b.

575 McGaughey, R. J.: FUSION/LDV: Software for LIDAR Data Analysis and Visualization,
576 <http://forsys.sefs.uw.edu/fusion/fusionlatest.html>, 2024.

577 Moran, C. J., Kane, V. R., and Seielstad, C. A.: Mapping forest canopy fuels in the western United States with
578 LiDAR-Landsat covariance, *Remote Sens.*, 12, <https://doi.org/10.3390/rs12061000>, 2020.

579 Mutlu, M., Popescu, S. C., Stripling, C., and Spencer, T.: Mapping surface fuel models using lidar and multispectral
580 data fusion for fire behavior, *Remote Sens. Environ.*, 112, 274–285, <https://doi.org/10.1016/j.rse.2007.05.005>, 2008.

581 Naesset, E.: Estimating above-ground biomass in young forests with airborne laser scanning, *Int. J. Remote Sens.*,
582 32, 473–501, <https://doi.org/http://www.tandfonline.com/doi/abs/10.1080/01431160903474970>, 2011.

583 Næsset, E.: Predicting forest stand characteristics with airborne scanning laser using a practical two-stage procedure
584 and field data, *Remote Sens. Environ.*, 80, 88–99, [https://doi.org/10.1016/S0034-4257\(01\)00290-5](https://doi.org/10.1016/S0034-4257(01)00290-5), 2002.

585 Næsset, E.: Practical large-scale forest stand inventory using a small-footprint airborne scanning laser, *Scand. J. For.
586 Res.*, 19, 164–179, <https://doi.org/10.1080/02827580310019257>, 2004.

587 Natural Resources Canada: The State of Canada’s Forests: Annual Report 2023, Natural Resources Canada,
588 Canadian Forest Service, Ottawa, Ontario., 116 pp., 2023.

589 Nelson, R.: How did we get here? An early history of forestry lidar, *Can. J. Remote Sens.*, 39, S6–S17,
590 <https://doi.org/10.5589/m13-011>, 2013.

591 Nelson, R., Gobakken, T., Næsset, E., Gregoire, T. G., Ståhl, G., Holm, S., and Flewelling, J.: Lidar sampling -
592 Using an airborne profiler to estimate forest biomass in Hedmark County, Norway, *Remote Sens. Environ.*, 123,
593 563–578, <https://doi.org/10.1016/j.rse.2011.10.036>, 2012.

594 Nilsson, M.: Estimation of tree heights and stand volume using an airborne lidar system, *Remote Sens. Environ.*, 56,

595 1–7, [https://doi.org/10.1016/0034-4257\(95\)00224-3](https://doi.org/10.1016/0034-4257(95)00224-3), 1996.

596 Ogle, S. M., Domke, G., Kurz, W. A., Rocha, M. T., Huffman, T., Swan, A., Smith, J. E., Woodall, C., and Krug,
597 T.: Delineating managed land for reporting national greenhouse gas emissions and removals to the United Nations
598 framework convention on climate change, *Carbon Balance Manag.*, 13,
599 <https://doi.org/https://doi.org/10.1186/s13021-018-0095-3>, 2018.

600 Parisien, M. A., Barber, Q. E., Hirsch, K. G., Stockdale, C. A., Erni, S., Wang, X., Arseneault, D., and Parks, S. A.:
601 Fire deficit increases wildfire risk for many communities in the Canadian boreal forest, *Nat. Commun.*, 11,
602 <https://doi.org/10.1038/s41467-020-15961-y>, 2020.

603 Parisien, M. A., Barber, Q. E., Flannigan, M. D., and Jain, P.: Broadleaf tree phenology and springtime wildfire
604 occurrence in boreal Canada, *Glob. Chang. Biol.*, 29, 6106–6119, <https://doi.org/10.1111/gcb.16820>, 2023.

605 Reutebuch, S. E., Anderson, H. E., and McGaughey, R. J.: Light detection and ranging (LIDAR): an emerging tool
606 for multiple resource inventory, *J. For.*, 103, 286–292, 2005.

607 Riaño, D., Meier, E., Allgöwer, B., Chuvieco, E., and Ustin, S. L.: Modeling airborne laser scanning data for the
608 spatial generation of critical forest parameters in fire behavior modeling, *Remote Sens. Environ.*, 86, 177–186,
609 [https://doi.org/10.1016/S0034-4257\(03\)00098-1](https://doi.org/10.1016/S0034-4257(03)00098-1), 2003.

610 Riaño, D., Chuvieco, E., Condés, S., González-Matesanz, J., and Ustin, S. L.: Generation of crown bulk density for
611 *Pinus sylvestris* L. from lidar, *Remote Sens. Environ.*, 92, 345–352, <https://doi.org/10.1016/j.rse.2003.12.014>, 2004.

612 Roussel, J. R. and Auty, D.: lidR: Airborne LiDAR Data Manipulation and Visualization for Forestry Applications,
613 <https://cran.r-project.org/package=lidR>, 2023.

614 Roussel, J. R., Auty, D., Coops, N. C., Tompalski, P., Goodbody, T. R. H., Meador, A. S., Bourdon, J. F., de
615 Boissieu, F., and Achim, A.: lidR: An R package for analysis of Airborne Laser Scanning (ALS) data, *Remote Sens.*
616 *Environ.*, 251, 112061, <https://doi.org/10.1016/j.rse.2020.112061>, 2020.

617 Shannon, C. E.: A mathematical theory of communication, *Bell Syst. Tech. J.*, 27, 379–423,
618 <https://doi.org/10.1002/j.1538-7305.1948.tb01338.x>, 1948.

619 Shi, Y., Wang, J., and Kissling, W. D.: Multi-temporal high-resolution data products of ecosystem structure derived
620 from country-wide airborne laser scanning surveys of the Netherlands, *Earth Syst. Sci. Data*, 17, 3641–3677,
621 <https://doi.org/10.5194/essd-17-3641-2025>, 2025.

622 Singh, K. K., Chen, G., Vogler, J. B., and Meentemeyer, R. K.: When big data are too much: effects of LiDAR
623 returns and point density on estimation of forest biomass, *IEEE J. Sel. Top. Appl. Earth Obs. Remote Sens.*, 9,
624 3210–3218, <https://doi.org/10.1109/JSTARS.2016.2522960>, 2016.

625 Solberg, S., Næsset, E., Hanssen, K. H., and Christiansen, E.: Mapping defoliation during a severe insect attack on

626 Scots pine using airborne laser scanning, *Remote Sens. Environ.*, 102, 364–376,
627 <https://doi.org/10.1016/j.rse.2006.03.001>, 2006.

628 Stefanidou, A., Gitas, I. Z., Korhonen, L., Stavrakoudis, D., and Georgopoulos, N.: LiDAR-based estimates of
629 canopy base height for a dense uneven-aged structured forest, *Remote Sens.*, 12, 1–20,
630 <https://doi.org/10.3390/rs12101565>, 2020.

631 Stinson, G., Thandi, G., Aitkin, D., Bailey, C., Boyd, J., Colley, M., Fraser, C., Gelhorn, L., Groenewegen, K.,
632 Hogg, A., Kapron, J., Leboeuf, A., Makar, M., Montigny, M., Pittman, B., Price, K., Salkeld, T., Smith, L.,
633 Viveiros, A., and Wilson, D.: A new approach for mapping forest management areas in Canada, *For. Chron.*, 95,
634 101–112, <https://doi.org/10.5558/tfc2019-017>, 2019.

635 Tews, J., Brose, U., Grimm, V., Tielbörger, K., Wichmann, M. C., Schwager, M., and Jeltsch, F.: Animal species
636 diversity driven by habitat heterogeneity/diversity: The importance of keystone structures, *J. Biogeogr.*, 31, 79–92,
637 <https://doi.org/10.1046/j.0305-0270.2003.00994.x>, 2004.

638 Tompalski, P.: *lidRmetrics*, <https://github.com/ptompalski/lidRmetrics>, 2024.

639 Tompalski, P., Hermosilla, T., Baral, S. K., Wulder, M. A., and White, J. C.: National remote sensing-derived
640 aboveground biomass yield curves for Canada, *For. An Int. J. For. Res.*, cpaf067,
641 <https://doi.org/10.1093/forestry/cpaf067>, 2025.

642 Vogelmann, J. E., Howard, S. M., Yang, L., Larson, C. R., Wylie, B. K., and VanDriel, N.: Completion of the 1990s
643 National Land Cover Data set for the conterminous United States from Landsat Thematic Mapper data and ancillary
644 data sources, *Photogramm. Eng. Remote Sensing*, June, 650–662, 2001.

645 Wells, J. V., Dawson, N., Culver, N., Reid, F. A., and Morgan Siegers, S.: The state of conservation in North
646 America’s Boreal Forest: issues and opportunities, *Front. For. Glob. Chang.*, 3, 1–18,
647 <https://doi.org/10.3389/ffgc.2020.00090>, 2020.

648 White, J. C., Wulder, M. A., Varhola, A., Vastaranta, M., Coops, N. C., Cook, B. D., Pitt, D., and Woods, M.: A
649 best practices guide for generating forest inventory attributes from airborne laser scanning data using an area-based
650 approach, Natural Resources Canada, Canadian Forest Service, Canadian Wood Fibre Centre, Information Report
651 FI-X-010, 50p. pp., 2013.

652 White, J. C., Wulder, M. A., Hobart, G. W., Luther, J. E., Hermosilla, T., Griffiths, P., Coops, N. C., Hall, R. J.,
653 Hostert, P., Dyk, A., and Guindon, L.: Pixel-based image compositing for large-area dense time series applications
654 and science, *Can. J. Remote Sens.*, 40, 192–212, <https://doi.org/10.1080/07038992.2014.945827>, 2014.

655 White, J. C., Tompalski, P., Vastaranta, M., Wulder, M. A., Saarinen, Stepper, C., and Coops, N. C.: A model
656 development and application guide for generating an enhanced forest inventory using airborne laser scanning data
657 and an area-based approach, [https://doi.org/DOI: 10.5558/tfc2013-132](https://doi.org/DOI:10.5558/tfc2013-132), 2017a.

658 White, J. C., Wulder, M. A., Hermosilla, T., Coops, N. C., and Hobart, G. W.: A nationwide annual characterization
659 of 25 years of forest disturbance and recovery for Canada using Landsat time series, *Remote Sens. Environ.*, 194,
660 303–321, <https://doi.org/10.1016/j.rse.2017.03.035>, 2017b.

661 White, J. C., Tompalski, P., Bater, C. W., Wulder, M. A., Fortin, M., Hennigar, C., Robere-McGugan, G., Sinclair,
662 I., and White, R.: Enhanced forest inventories in Canada: implementation, status, and research needs, *Can. J. For.*
663 *Res.*, 55, 1–37, <https://doi.org/10.1139/cjfr-2024-0255>, 2025.

664 Woods, M., Lim, K., and Treitz, P.: Predicting forest stand variables from LiDAR data in the Great Lakes - St.
665 Lawrence forest of Ontario, *For. Chron.*, 84, 827–839, 2008.

666 Wulder, M. A., Bater, C. W., Coops, N. C., Hilker, T., and White, J. C.: The role of LiDAR in sustainable forest
667 management, *For. Chron.*, 84, 807–826, <https://doi.org/10.5558/tfc84807-6>, 2008.

668 Wulder, M. A., White, J. C., Bater, C. W., Coops, N. C., Hopkinson, C., and Chen, G.: Lidar plots — a new large-
669 area data collection option: context, concepts, and case study, *Can. J. Remote Sens.*, 38, 600–618,
670 <https://doi.org/10.5589/m12-049>, 2012a.

671 Wulder, M. A., White, J. C., Nelson, R. F., Næsset, E., Ørka, H. O., Coops, N. C., Hilker, T., Bater, C. W., and
672 Gobakken, T.: Lidar sampling for large-area forest characterization: A review, *Remote Sens. Environ.*, 121, 196–
673 209, <https://doi.org/10.1016/j.rse.2012.02.001>, 2012b.

674 Wulder, M. A., Hermosilla, T., White, J. C., Bater, C. W., Hobart, G., and Bronson, S. C.: Development and
675 implementation of a stand-level satellite-based forest inventory for Canada, *For. An Int. J. For. Res.*, 97, 546–563,
676 <https://doi.org/10.1093/forestry/cpad065>, 2024.

677 Zald, H. S. J., Wulder, M. A., White, J. C., Hilker, T., Hermosilla, T., Hobart, G. W., and Coops, N. C.: Integrating
678 Landsat pixel composites and change metrics with lidar plots to predictively map forest structure and aboveground
679 biomass in Saskatchewan, Canada, *Remote Sens. Environ.*, 176, 188–201, <https://doi.org/10.1016/j.rse.2016.01.015>,
680 2016.

681